analytical chemistry

Article

Cite This: Anal. Chem. 2018, 90, 11614−11621

pubs.acs.org/ac

Composition-Tunable Hollow Au/Ag SERS Nanoprobes Coupled with Target-Catalyzed Hairpin Assembly for Triple-Amplification Detection of miRNA

Yudie Sun and Tao Li*

Department of Chemistry, University of Science & Technology of China, Hefei, Anhui 230026, China

Supporting Information

ABSTRACT: Detecting disease-related biomarkers is of great significance for disease diagnosis and therapy. In this work, we develop an ultrasensitive surface-enhanced Raman scattering (SERS) biosensor for the detection of an acute myocardial infarction-related miRNA (miR-133a) using composition-adjustable hollow Ag/Au nanosphere-based SERS probes coupled with the target-catalyzed hairpin assembly (CHA) strategy. Bimetallic probes displaying high stability and a strong surface plasmon resonance effect were synthesized with a controllable ratio of silver and gold by a galvanic replacement method and then captured by a duplex linker produced in the CHA process to accomplish signal amplification. In this way, the target miR-133a can be detected in a wide linear range with a detection limit of 0.306 fM and high selectivity over other miRNAs expressed in human hearts. Practical applications in human blood samples reveal the strong anti-interference ability and ideal sensitivity of our developed sensing platform in physiological environments, benefiting its potential biomedical applications.

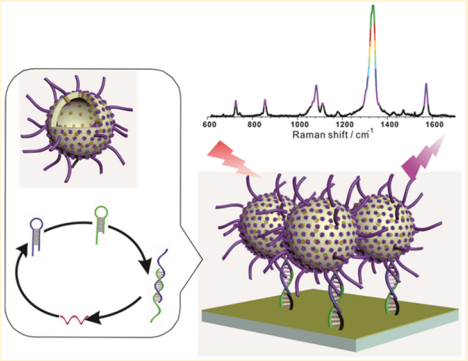

Acute myocardial infarction (AMI) is a severe cardiovascular event. Prolonged ischemia will cause death of myocardial tissue and even lead to heart failure.[1−3] Consequently, precise analysis of AMI-related biomarkers for diagnosis and therapy is highly clinically relevant. A large number of studies have demonstrated that miRNAs are closely related to the fate of the heart because they can regulate the death and regeneration of cardiac cells after AMI.[4−7] Thus, it is of significance to develop sensitive and specific methods for the analysis of heart-associated miRNAs.

Up to now, much effort has been devoted to sensitively analyzing miRNA with different strategies and techniques, including a DNAzyme-assisted fluorescence signal amplification method,[8−11] a nanoparticle assembly-induced SPR enhancement technique,[12−14] nucleic acid-assisted signal amplification,[15,16] an enzyme-boosted SERS signal amplification strategy,[17] and single-stranded RNA sequencing by tip-enhanced Raman spectroscopy (TERS).[18] Among them, Raman spectroscopy is one of the most powerful spectroscopic tools for bioassay and life science owing to its high sensitivity, specific fingerprints, and fast data acquisition speed.[19−23] Though TERS exhibits several advantages over SERS, such as excellent spatial resolution, single molecule detection, and short acquisition time, it is not suitable for quantitative analysis.[24] Recently, several SERS detection platforms for assays of miRNA have been developed.[25−28] However, unlike cancers and other miRNA-involved diseases, the actual environment of the heart is more complex than that of cells. Because there exist multiple cell types, unnecessary expression of diversified miRNA and low content of target miRNA are inevitable in the patients' blood.[29−31] Furthermore, a variety of disrupters in blood make miRNAs more susceptible to be degraded. Therefore, there are few reports on the sensitive SERS detection of AMI-related miRNAs especially in heart-mimicking environments.

Because electromagnetic enhancement is the main enhancement mechanism of SERS, the probe for SERS-based biological analyses plays a critical role in improving SERS sensitivity and reproducibility. Therefore, synthesis of SERS-active nanostructures for designing SERS probes with strong electromagnetic enhancement effect and good stability is an important procedure toward realizing reliable assay of miRNAs. Compared with solid noble metal materials, their corresponding counterparts with cavities usually possess superior SERS activity.[32−34] It is also obvious that hollow nanoparticles possess lower density and will be better dispersed without precipitation for a long time, and this superiority may also make it easier to facilitate biosensing reactions. Given their advantages of cavity-enhanced activity[32−34] and high biocompatibility,[3,35,36] hollow Ag/Au bimetallic nanospheres were synthesized here with a controllable ratio of silver and gold by a galvanic replacement method,[3,37] as shown in Scheme 1a. To our knowledge, such SERS probes using hollow Au/Ag nanospheres with suitable size and optimal composition to generate turn-on SERS signal for quantitative detection of target miRNA are rather rarely reported.[3,38,39] The ratio of

Received: July 9, 2018
Accepted: September 3, 2018
Published: September 3, 2018

DOI: 10.1021/acs.analchem.8b03067
Anal. Chem. 2018, 90, 11614−11621

Scheme 1. (a) Preparation Strategy of SERS Probes. (b) Target-Catalyzed Hairpin Assembly (CHA) Process. (c) Final Structure for the SERS Detection Platform

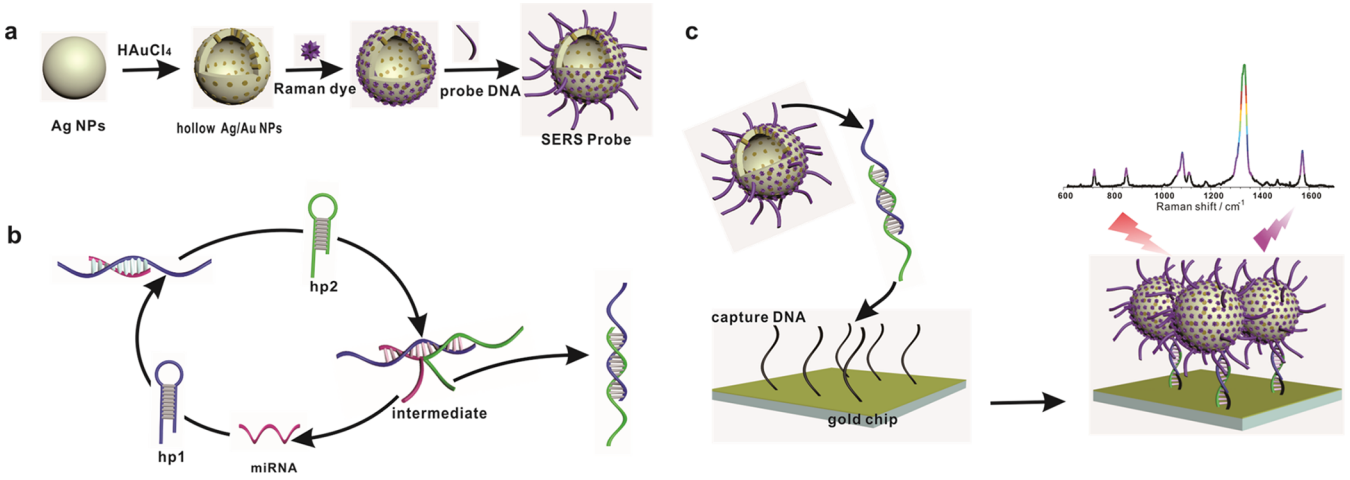

elemental composition can be adjusted, and they distribute homogeneously at atomic level. Strongly coupled SPR from both inner and outer surfaces of the cavity wall, as well as homogeneous element distribution, endows the hollow Ag/Au nanospheres with numerous SERS hot spots, as reported recently.[40]

Unlike most previous counterparts[25,41−45] in which the target miRNAs are directly used as linkers to capture the SERS probes in a sandwich mode, we adopted a duplex linker with two sticking ends produced in the target-catalyzed hairpin assembly (CHA) process (Scheme 1b). Accordingly, the hollow probe was attached onto an islanded gold chip[46] (Scheme 1c). This design can not only achieve triple signal amplification via the bimetallic cavity, CHA, and gold islands but can also prevent the structural damage usually occurring in sandwich-type assays.[47] By CHA strategy, the probes can be separated by a gold chip through complementary double-stranded DNA rather than a complementary strand of RNA and DNA, which are easily degradable. In this way, we have made some progress in sandwich-type SERS detection of miRNA. Such a strategy combined with sensitive SERS probes enables the ultrasensitive and selective detection of an acute myocardial infarction-related miRNA (miR-133a), endowing our developed sensing platform with a strong anti-interference ability in real blood samples.

EXPERIMENTAL SECTION

Materials and Reagents. All qualified DNA oligonucleotides were purchased from Sangon Biological Engineering Technology & Services Co., Ltd. (Shanghai, China). All purified miRNAs were purchased from Gene Pharma RNA Co., Ltd. (Shanghai, China). All used sequences of nucleic acids are listed in Table S1. Diethyl pyrocarbonate (DEPC)−water and RNase inhibitor were purchased from Sangon Biological Engineering Technology & Services Co., Ltd. Then all solutions were treated with 0.1% DEPC followed by autoclaving. Sodium borohydride ($NaBH_4$), magnesium acetate ($MgAc_2$), chloroauric acid ($HAuCl_4$), sodium chloride (NaCl), and hydroxylamine hydrochloride ($NH_2OH{\cdot}HCl$) were provided by Sinopharm Chemical Reagent Co., Ltd. (China). SH-PEG-350, 4-nitrothiophenol (NBT), tris(2-carboxyethyl)phosphine hydrochloride (TCEP), and Tween-20 were purchased from Sigma−Aldrich Co., Ltd. (Shanghai,-China). All of the chemicals used in this study were analytical grade. Ultrapure water (>18.2 MΩ·cm) was produced by a Millipore Milli-Q gradient system. Human serum was extracted by the First Affiliated Hospital of Nanjing Medical University.

Instrumentation. Scanning electron microscopy (SEM) images were scanned by field-emission SEM (JEOL JSM-6700F, 0 kV). Structural characterization of the hollow Ag/Au nanospheres was performed with a UV−vis spectrometer (Cary 60) and transmission electron microscope (Hitachi H-7650). The element mapping of Ag/Au nanospheres was characterized by a high-resolution transmission electron microscope (Talos F200X). The gel electrophoresis results were exposed by a Tanon Gel Images System (Tanon-1600). Raman measurements were taken with a He−Ne laser Raman microscope (inVia, Renishaw, West Dundee, IL, 785 nm, 5 mW) .

Synthesis of Plasmonic Chips. Plasmonic gold chips were synthesized as in our previous research.[48] Briefly, glass slides were immersed in 5 mM $HAuCl_4$ solution, followed by adding 200 μL of ammonium hydroxide and then shaking for 1 min immediately. After washing, 1 mM $NaBH_4$ solution was added to form gold nanoparticle seeds. Finally, the synthesis was completed by incubating the chip in a mixture of 0.5 mM hydroxylamine and 0.5 mM $HAuCl_4$. The detection reactors were made by coating the chip with polydimethylsiloxane (PDMS) film, which was punched with holes (4 mm in diameter). The enhancement factor (EF) of the gold substrate was calculated to be 2.4×10^6 on the basis of SERS intensity of NBT (Figure S1).

Synthesis of Hollow Au/Ag Nanospheres. Silver nanoparticles were first prepared by reducing silver nitrate with sodium citrate. In brief, 200 mL of 0.1 mM aqueous $AgNO_2$ was heated to boiling, and then 4 mL of 0.1 M $C_6H_5Na_3O_7{\cdot}2H_2O$ was added rapidly. The solution was kept boiling for 1 h, and the color changed to green-yellow, indicating the formation of AgNPs. Next, the temperature of the resulting solution was controlled at 88 °C for galvanic replacement reaction. To form the hollow structures, 1 mM $HAuCl_4$ solution was dropped into the AgNP solution every three seconds. With the increasing amount of $HAuCl_4$, the solution changed to a different color and finally turned red. Nanoparticles with a different color were sucked out for characterization and application.

DOI: 10.1021/acs.analchem.8b03067
Anal. Chem. 2018, 90, 11614−11621

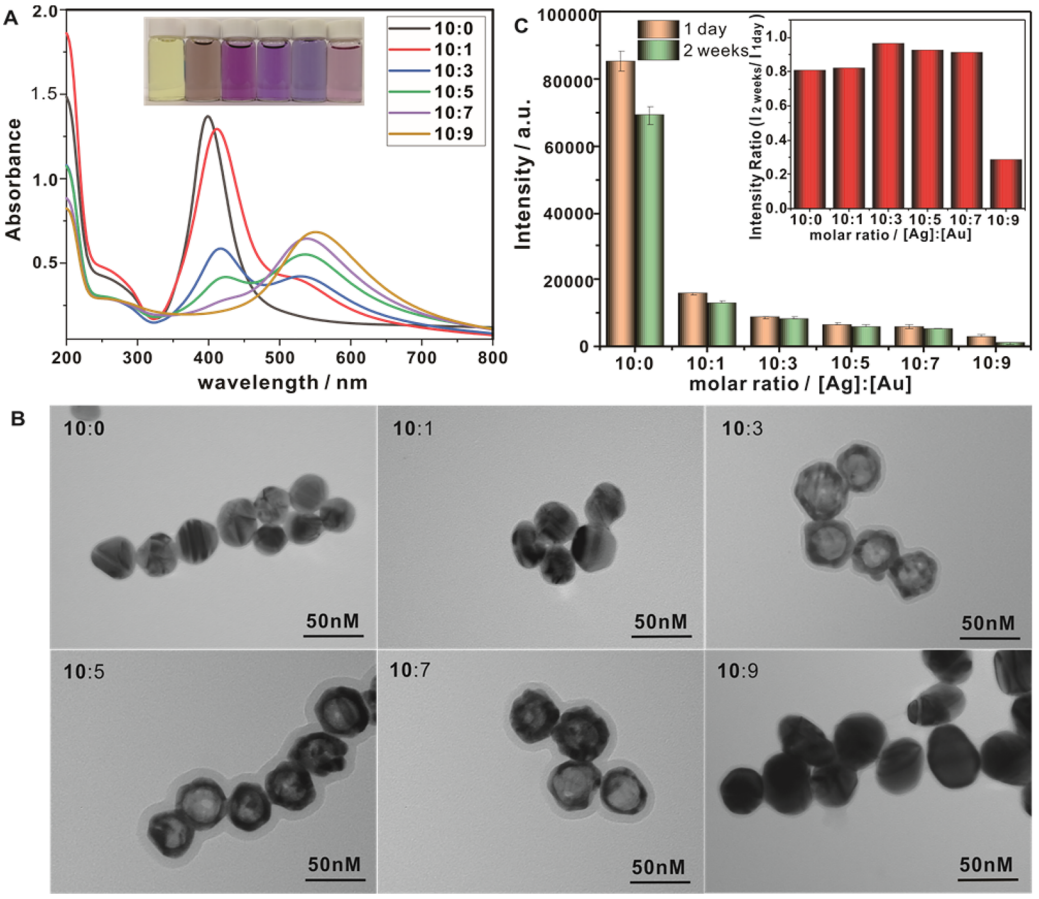

Figure 1. Characterization of the structures prepared under different $[Ag^+]/[Au^{3+}]$ values. (A) UV−vis spectra corresponding to nanoparticles synthesized at different ratios of $[Ag^+]/[Au^{3+}]$. (B) TEM images of nanostructures formed under different $[Ag^+]/[Au^+]$ values. (C) Raman signal intensities at 1335 cm^{-1} for nanoparticles formed at different $[Ag^+]/[Au^{3+}]$ values on the first day and after storage for 2 weeks at 4 °C in a glass bottle. Inset: the ratio of intensity at 2 weeks to intensity at the first day.

Procedure for SERS Probes. The SERS probes were made by assembling NBT-coated hollow Au/Ag nanospheres with capture DNAs. First, hollow Au/Ag nanospheres (1 nM, 2 mL) were stirred with 10 μM NBT for 4 h at room temperature. After washing, the Raman dye-encoded hollow Au/Ag nanospheres were incubated with the capture DNAs (100 μM, 30 μL) for 6 h at room temperature. Next, 1 M NaCl was added into the mixtures every 0.5 h to a final concentration of 0.1 M NaCl and stored overnight. Subsequently, the probes were washed multiple times with PBS buffer and finally redispersed in PBS buffer. Finally, the prepared SERS probes were stored at 4 °C for later use.

Polyacrylamide Gel Electrophoresis (PAGE). Hairpin DNA were formed by annealing at 90 °C for 10 min, followed by air cooling to room temperature. Different concentrations of miR-133a were added into 20 μL of solution (2 mM $MgAc_2$, 100 mM NaAc) which consisted of 0.5 μM hp1 and 0.5 μM hp2 and then incubated at 37 °C for 2 h. The miRNA-boosted results of the DNA molecular machine were analyzed by polyacrylamide gel electrophoresis (10%, w/w) with 100 mM NaAc and 2 mM $MgAc_2$ in 1× TA buffer at 32 V for 10 h.

miRNA Detection Technique. RNA detection was performed in the PDMS reactor. The chip was modified with thiolated DNA (20 μL, 3 μM) in 10 mM PBS buffer (pH 7.4, 1 M NaCl) for 4 h at 25 °C. After washing, 20 μL of 100 μM S-PEG-350 was added and washed after storing for 30 min. Before SERS detection, the DNA molecular machine was first triggered by incubating different concentrations of miRNA with 2 μM hp1 and 2 μM hp2 at 37 °C for 2 h. The reaction solution and 5 μL of SERS probe were added into the PDMS reactor and kept for 3 h at room temperature. Finally, the chip was washed with 0.1% (w/v) Tween in PB buffer three times to remove extra probes and dried.

RESULTS AND DISCUSSION

Preparation and Characterization of Hollow Au/Ag Bimetallic SERS Probes. The synthesis process for hollow Au/Ag nanospheres is described in Scheme 1a. The synthesized nanospheres are functionalized with NBT and probe DNA that hybridizes with one sticking end of the duplex linker produced in the CHA process (Scheme 1b). The SERS probe can be attached onto the detection substrate via hybridizing another sticking end of the duplex linker with the capture DNA (Scheme 1c).

Figure 1A shows the UV−vis spectra of the nanoparticles prepared under different values of $[Ag^+]/[Au^{3+}]$. Initially, only a peak corresponding to Ag at 400 nm is observed. Upon addition of Au^{3+}, a new localized surface plasmon resonance (LSPR) peak appears around 532 nm, which can be assigned to Au. With the increasing molar ratio of $[Au^{3+}]$, the peak at 400 nm decreases gradually, while the peak at 532 nm increases and is red-shifted. With the ratio of $[Ag^+]/[Au^{3+}]$ increasing to 10:9, the LSPR peaks at 400 nm disappeared. These results indicate that with the increasing amount of Au^{3+},

DOI: 10.1021/acs.analchem.8b03067
Anal. Chem. 2018, 90, 11614−11621

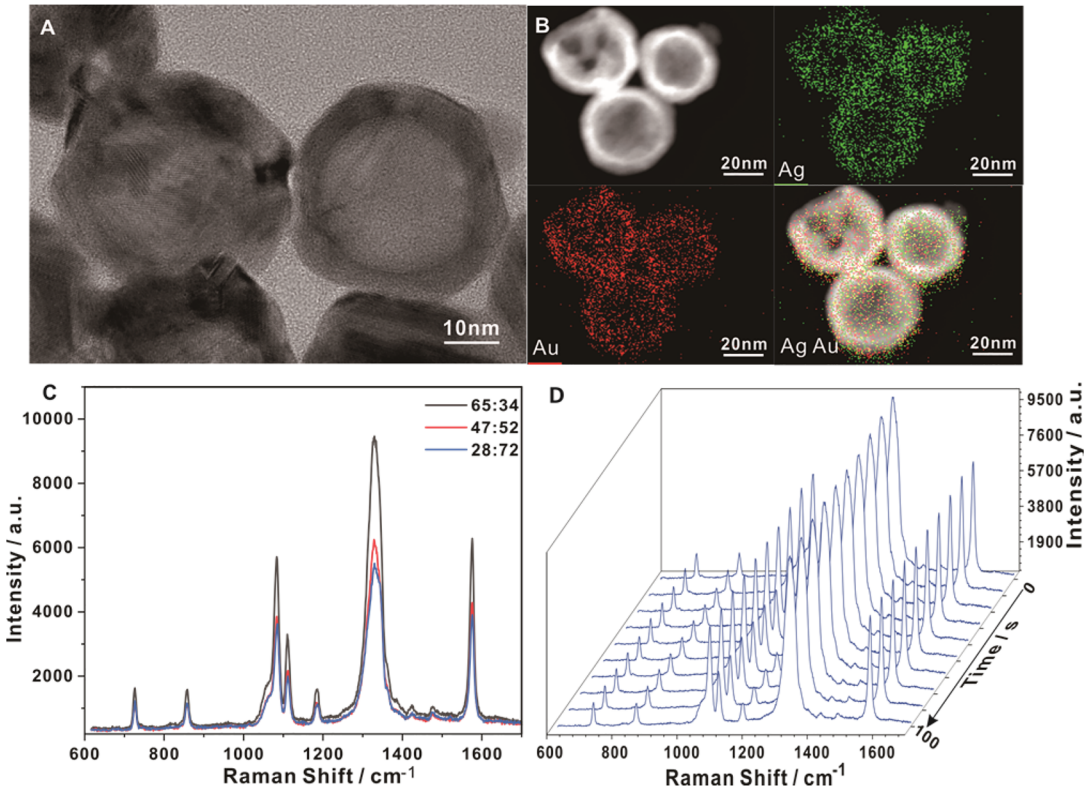

Figure 2. Characterization of the optimal hollow Au/Ag nanospheres synthesized with $[Ag^+]/[Au^{3+}]$ = 10:3. (A) HRTEM images. (B) EDX elemental mapping images. (C) SERS spectra 0f NBT (10^{-6} M) corresponding to hollow Au/Ag nanospheres with different Ag and Au atomic ratios. (D) Time-dependent Raman results of the hollow Au/Ag nanospheres when the content of Au atoms is 34%.

more and more Ag is replaced, consistent with previous observations.[40] Moreover, the corresponding TEM images reveal the existence of a central cavity in the nanosphere (Figure 1B) in the case of $[Ag^+]/[Au^{3+}]$ = 10:3, and such a hollow structure remains unchanged even with the ratio increasing to 10:7. As the ratio further increases to 10:9, the cavities disappear and some solid anomalous spherical nanostructures emerge.

To optimize performance of the SERS assay, SERS studies of both perspectives of intensity and stability are needed. The Raman responses of nanoparticles synthesized under varying values of $[Ag^+]/[Au^{3+}]$ were studied, and the fingerprint peaks of NBT at 1335 cm^{-1} were used for comparison. As shown in Figure 1C, the strongest SERS signal occurs at $[Ag^+]/[Au^{3+}]$ = 10:0, and the signal gradually decreases as the ratio increases, mainly attributed to the strong plasmonic enhancement effect of silver.[49] However, it is clearly observed that the signal corresponding to pure silver nanoparticles, the second ratio product, and the last one decreases significantly after 2 weeks. Furthermore, we found alot of small particles in the silver solution, and most of them adhere to the surface of the silver nanoparticles after 2 weeks (Figure S4). We speculate that the silver particles had disintegrated because the active chemical property of silver and high density caused instability of the solid nanoparticles.[50,51] Thus, the signal decrease may be caused by morphologic change of the silver particles, indicating their instability and poor anti-interference ability. In contrast, no changes take place for the 10:3 Ag/Au structure. The inset in Figure 1C illustrates the intensity ratio of the two time periods. The hollow structures demonstrate stability higher than that of the solid structures, and the hollow nanospheres synthesized at the ratio $[Ag^+]/[Au^{3+}]$ = 10:3 display the best stability and the strongest SERS signal among all hollow structures. For these reasons, we chose the 10:3 Ag/Au structure as the SERS probe to resist multiple disturbances in real samples for biosensing, even at the cost of signal reduction compared to simple Ag particles.

In consideration of the analysis results, we further investigated the properties of hollow Au/Ag nanospheres synthesized with $[Ag^+]/[Au^{3+}]$ = 10:3. From the high-resolution TEM (HRTEM) images in Figure 2A, the hollow interiors of Au/Ag nanospheres are clearly observed. The SEM images in Figure S2D also illustrate that the hollow Ag/Au nanospheres could be synthesized in high yield and excellent uniformity. By EDS mapping analysis, we find Ag and Au elements distribute uniformly in the shell of hollow Au/Ag nanospheres (Figure 2B), which lays a foundation for generating uniform hot spots.[52] We also investigated the morphology and element distribution of other hollow spheres formed under different $[Ag^+]/[Au^{3+}]$ values by SEM and EDX mapping analysis. The results illustrate that with a variable ratio of $[Ag^+]/[Au^{3+}]$, the content of Ag and Au atoms in the shell are successfully adjusted, as shown in Figures S2G–S2I. The elemental mappings (Figure S2A–S2C) clearly show that Ag and Au distribute homogeneously on the shell of all hollow nanospheres with different atom ratios. From the dynamic light scattering measurement, the mean particle size determined by number was 43 ± 7 nm (Figure S5). The XRD pattern further demonstrates that the hollow Au/Ag nanospheres are formed with silver and gold (Figure S6). The analysis results demonstrate that we can tune the composition of hollow Au/Ag nanospheres to regulate the quantity of the uniform distributed hot spots.

DOI: 10.1021/acs.analchem.8b03067
Anal. Chem. 2018, 90, 11614–11621

Figure 2C shows that the characteristic peak of the Raman dye remains as the percentage of Au atom increases, but the SERS intensity decreases gradually. Then time-dependent Raman spectra of the hollow Au/Ag nanospheres with 34% Au atoms indicates that the hollow structures can produce highly uniform and reproducible SERS signals for detection. According to the above observations, hollow bimetallic nanospheres with $[Ag^+]/[Au^{3+}]$ = 10:3 are chosen as SERS probes, of which the content of Au atoms is 34%.

Ultrasensitive SERS Sensor for miRNA Coupled with CHA. As described in Scheme 1, the above-synthesized nanospherical probes are utilized for SERS detection of the target miRNA that triggers the CHA reaction. Here miR-133a is adopted, which is a 22-nt RNA highly expressed in the AMI patients' blood and holds great promise for in vitro diagnosis.[2] In the CHA process, two component DNA hairpins (hp1 and hp2) are first analyzed by NUPACK to predict their conformations and final CHA products (Figure S3). The CHA reaction starts from the hybridization of miR-133a with hp1 whose 5′ end contains a complementary sequence of the probe DNA attached on SERS probes. Furthermore, the other two regions of hp1 are composed of the antisense strand of miR-133a and a trigger sequence for hp2 at the 3′ end. Hybridization with miR-133a can open hp1 via toehold-mediated strand displacement (TMSD) and expose the trigger region, which continues to open hp2 via the TMSD reaction, and finally miR-133a is replaced, thereby participating in the next cycle (Scheme 1b). As the final product of CHA, a duplex linker with two sticking ends allows SERS probes to be anchored onto gold islands via hybridization with the probe and capture DNAs (Scheme 1c). By these means, ultrasensitive SERS analysis of the target miRNA is expected due to the triple-enhancement effect from the hollow Ag/Au SERS probe, plasmonic substrate with multiple hot spots, and the CHA signal amplification.

We employed native PAGE to verify that the CHA process occurs as we designed (Figure 3). It shows that hp1 and hp2 are kept stable in the absence of miR-133a (lane 5). Upon addition of miR-133a, a new band moving slower than those of hp1 and hp2 appears. As the concentration of miR-133a increases, the new band becomes clearer gradually, accompanied by the disappearance of the hp1 and hp2 mixture (lanes 6−8). This suggests that hp1 and hp2 are consumed to form the expected product (Scheme 1b). This resulting structure is next employed as a linker, immobilizing the probe onto the substrate in SERS assays.

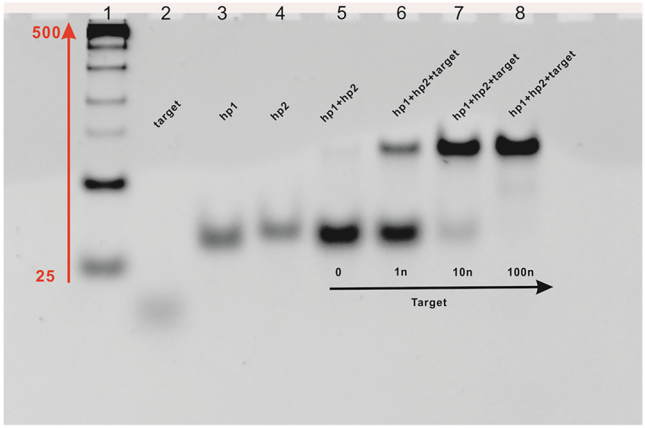

Figure 3. Polyacrylamide gel electrophoresis results of the miR-133a-powered DNA molecular machine. Lanes 1−8: marker, miR-133a, hp1, hp2, hp1 + hp2, hp1 + hp2 + 1 nM miR-133a, hp1 + hp2 + 10 nM miR-133a, hp1 + hp2 + 100 nM miR-133a. The total volume of all samples was 20 μL, and the concentration of DNA was 0.5 μM.

Figure 4A depicts the SERS spectra for the analysis of different concentrations of miR-133a. With the increasing concentration of miR-133a, the intensity of SERS peaks from Raman dyes (NBT) increases progressively. By comparing with the blank spectrum, it is observed that 1 fM miR-133a can cause a remarkable change in SERS signal, indicating a lowest detectable concentration (LDC) of 1 fM for miR-133a analysis. For quantitative study, the intensities of the Raman peak at 1335 cm^{-1} are plotted as a function of the logarithm of miR-133a concentration. The calibration curve in Figure 4B shows a wide linear relationship in the range of 1 fM to 10 nM for our SERS biosensing platform, with a limit of detection (LOD) of 0.306 fM (S/N = 3). Our resulting detection range/limit is not only superior to most of the sandwich-type SERS sensors for the detection of nucleic acids but also better than most of the CHA strategy-based miRNA detection using different techniques (Tables S2 and S3). In addition, by comparison with other sandwich-type SERS assays, our strategy is cost-effective and sensitive (Table S2). Although the assay time of our platform is not the best, taking the detection results, fabrication time, cost, and assay time into consideration, our platform is more practical than other sandwich-type SERS sensors.

Furthermore, parallel experiments were performed to test the selectivity of our sensing platform for miR-133a over other AMI-related miRNAs (miR-499, miR-208, and miR-328) that coexist in blood.[53] For each measurement, the reaction conditions are the same as that of miR-133a, except for a 1000-fold higher concentration of coexisted miRNAs. Figure 4C exhibits the spectra for four individual miRNAs and their mixtures, respectively. From the spectra we can find that the SERS signals are detectable only in the presence of miRNAs, and the interfering miRNAs result in no observable change in the background signal. Figure 4D shows a comparison between the intensity of 1335 cm^{-1} for miR-499, miR-208, miR-328, and miR-133a and their mixtures with the blank sample, demonstrating that our developed sensing platform responds well to the target miR-133a, independent of the coexistence of interfering miRNAs. Thus, a good selectivity is achieved. The reliability of the SERS sensor was further tested via collection from random spots on the chip (Figure 4E), and their intensities show little variation by quantitative analysis of the characteristic peak at 1335 cm^{-1} (Figure 4F). A high reproducibility of data is observed. These results reveal a good reliability of our developed sensing platform. Therefore, this ultrasensitive biosensor holds great potential for assay of AMI-related miRNAs in complex cardiac systems.

SERS Assay for Serum Samples. Currently, the LOD of our method is not as sensitive as other methods, but it still shows significant potential as a reliable and sensitive sensor for miRNA in some complicated scenarios such as myocardial disease, blood disease, and liver cancer. Our method may be suitable for acute myocardial infarction; however, this effort has been hampered due to the availability of patients' blood with research value. Serum is another important research challenge that should be explored, because it contains significant barriers for the diagnosis of AMI. In serum there is a variety of proteins, enzymes, ions, etc., and these

DOI: 10.1021/acs.analchem.8b03067
Anal. Chem. 2018, 90, 11614−11621

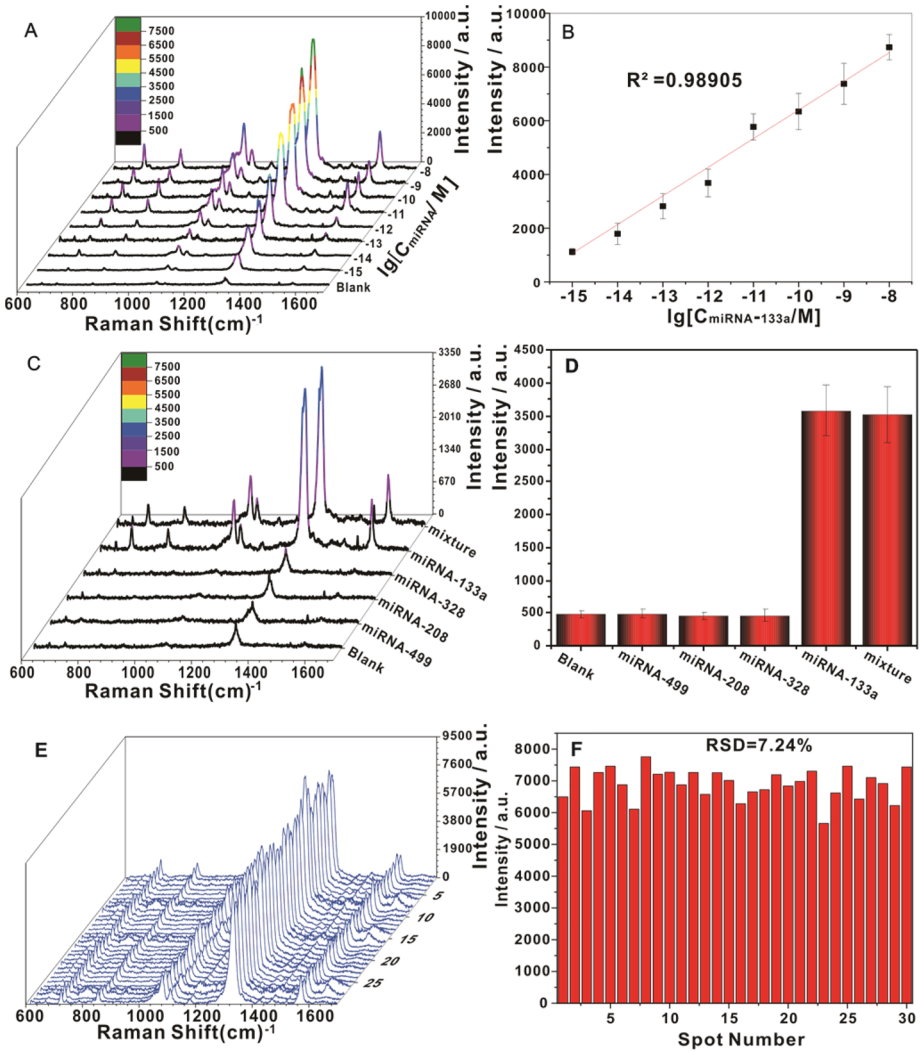

Figure 4. SERS assay performance for miRNA detection. (A) Representative SERS spectra corresponding to miR-133a with varying concentrations. (B) Standard curve of SERS intensity (I1335) as a function of miR-133a concentration. (C) SERS spectra and (D) SERS intensities at 1335 cm^{-1} of specific analyses for noncomplementary miRNAs (miR-499, miR-208, and miR-328) and a mixture of all the four miRNAs. Error bar represents the standard deviation of different batches (n = 3). The concentrations of noncomplementary miRNAs were 1 nM, and the concentrations of target miRNAs were 1 pM. (E) SERS spectra and (F) Raman intensities at 1335 cm^{-1} obtained from 30 random spots. The concentration of miR-133a is 1 nM.

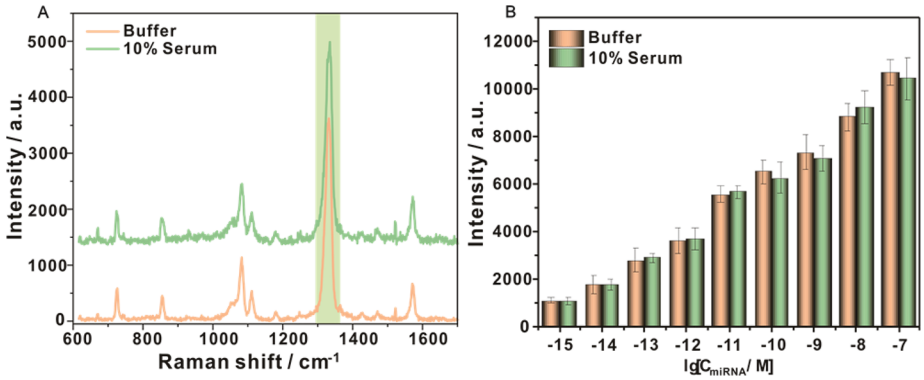

Figure 5. (A) SERS spectrum for detection of 1 pM miR-133a in buffer and in diluted (10%) serum. (B) SERS intensities at 1335 cm^{-1} when testing miR-133a in buffer and in diluted (10%) serum. Data were collected from three batches.

interfering components cause miRNAs to be hydrolyzed much easier and the sensitivity of the method may be reduced.

Practical applications of our SERS sensor were tested by detecting the target miRNA in real serum samples (Figure 5). By comparing the SERS spectrum obtained from buffer and 10% human serum in Figure 5A, we find that there are no significant differences in both intensity and characteristic peaks. Due to the strong anti-interference ability of the hollow

DOI: 10.1021/acs.analchem.8b03067
Anal. Chem. 2018, 90, 11614−11621

Ag/Au bimetallic SERS probes and the amplification effect of the CHA process, interfering molecules in the serum have no effect on the SERS detection. Quantitative investigations for miR-133a ranging from 1 fM to 10 nM in buffer and 10% human serum are basically the same (Figure 5B). Thus, the application in real sample analysis is coincident with the theoretical model, which indicates that the SERS detection strategy holds great potential for diagnosing AMI.

CONCLUSIONS

A CHA-assisted ultrasensitive sandwich-type miRNA detection platform has been developed using composition-adjustable hollow Ag/Au bimetallic nanospheres as SERS probes. Taking advantage of the CHA signal amplification and cavity-enhanced activity of the hollow Ag/Au SERS probes, an LDC of 1 fM and LOD of 0.306 fM for AMI-related miRNA have been achieved, with a wide linear range superior to previous counterparts.[25,28,41−43] However, because our strategy involves multiple reactions and washing steps, the sensitivity may be sacrificed to some extent and longer times are needed. Nonetheless, the detection platform holds great application prospects in biosensing and disease diagnosis. By adjusting the sequences of CHA components, our detection platform may be extended to the detection of various genes and presents a general way to develop diverse SERS sensors for different applications.

ASSOCIATED CONTENT

Supporting Information

The Supporting Information is available free of charge on the ACS Publications website at DOI: 10.1021/acs.analchem.8b03067.

SEM images for plasmonic chip. The optimal conformation and free energy of secondary structure. Characterization of the hollow Au/Ag nanospheres synthesized with different ratios of $[Ag^+]/[Au^{3+}]$. Sequences of oligonucleotide used in this study. Comparison of the sandwich-type SERS sensors for the detection of nucleic acids (PDF)

AUTHOR INFORMATION

Corresponding Author

*Fax: (+86)551-63601813. E-mail: tlitao@ustc.edu.cn.

ORCID

Yudie Sun: 0000-0002-1053-7472

Tao Li: 0000-0002-9724-3812

Notes

The authors declare no competing financial interest.

ACKNOWLEDGMENTS

We thank Zefeng Hua, Qiwei Wang, Ruiyan Guo, and Jiao Zheng for their help in our study. This work was supported by the National Key Research and Development Program of China [no. 2016YFA0201300], the National Natural Science Foundation of China [no. 21575133], and the Recruitment Program of Global Experts.

REFERENCES

(1) Wang, K.; Liu, C. Y.; Zhou, L. Y.; Wang, J. X.; Wang, M.; Zhao, B.; Zhao, W. K.; Xu, S. J.; Fan, L. H.; Zhang, X. J.; Feng, C.; Wang, C. Q.; Zhao, Y. F.; Li, P. F. *Nat. Commun.* **2015**, *6*, 6779.

(2) Boon, R. A.; Dimmeler, S. *Nat. Rev. Cardiol.* **2015**, *12*, 135.

(3) Choi, Y.; Hong, S.; Liu, L.; Kim, S. K.; Park, S. *Langmuir* **2012**, *28* (16), 6670−6.

(4) Wang, J.; Huang, W.; Xu, R.; Nie, Y.; Cao, X.; Meng, J.; Xu, X.; Hu, S.; Zheng, Z. *J. Cell. Mol. Med.* **2012**, *16* (9), 2150−60.

(5) Sun, T.; Dong, Y.-H.; Du, W.; Shi, C.-Y.; Wang, K.; Tariq, M.-A.; Wang, J.-X.; Li, P.-F. *Int. J. Mol. Sci.* **2017**, *18* (4), 745.

(6) Fiedler, J.; Thum, T. *Arterioscler., Thromb., Vasc. Biol.* **2013**, *33* (2), 201−5.

(7) Ottersbach, A.; Mykhaylyk, O.; Heidsieck, A.; Eberbeck, D.; Rieck, S.; Zimmermann, K.; Breitbach, M.; Engelbrecht, B.; Brügmann, T.; Hesse, M.; et al. *Biomaterials* **2018**, *155*, 176−190.

(8) Chen, F.; Bai, M.; Cao, K.; Zhao, Y.; Cao, X.; Wei, J.; Wu, N.; Li, J.; Wang, L.; Fan, C.; Zhao, Y. *ACS Nano* **2017**, *11* (12), 11908−11914.

(9) Bakshi, S. F.; Guz, N.; Zakharchenko, A.; Deng, H.; Tumanov, A. V.; Woodworth, C. D.; Minko, S.; Kolpashchikov, D. M.; Katz, E. *Nanoscale* **2018**, *10* (3), 1356−1365.

(10) Ying, Z. M.; Wu, Z.; Tu, B.; Tan, W.; Jiang, J. H. *J. Am. Chem. Soc.* **2017**, *139* (29), 9779−9782.

(11) Bakshi, S. F.; Guz, N.; Zakharchenko, A.; Deng, H.; Tumanov, A. V.; Woodworth, C. D.; Minko, S.; Kolpashchikov, D. M.; Katz, E. *J. Am. Chem. Soc.* **2017**, *139* (35), 12117−12120.

(12) Zhou, W.; Li, Q.; Liu, H.; Yang, J.; Liu, D. *ACS Nano* **2017**, *11* (4), 3532−3541.

(13) Zhang, K.; Yang, L.; Lu, F.; Wu, X.; Zhu, J. J. *Small* **2018**, *14* (10), 1703858.

(14) Ma, W.; Fu, P.; Sun, M.; Xu, L.; Kuang, H.; Xu, C. *J. Am. Chem. Soc.* **2017**, *139* (34), 11752−11759.

(15) Liang, C. P.; Ma, P. Q.; Liu, H.; Guo, X.; Yin, B. C.; Ye, B. C. *Angew. Chem., Int. Ed.* **2017**, *56* (31), 9077−9081.

(16) He, L.; Lu, D.; Liang, H.; Xie, S.; Zhang, X.; Liu, Q.; Yuan, Q.; Tan, W. *J. Am. Chem. Soc.* **2018**, *140* (1), 258−263.

(17) Li, Y.; Zhao, Q.; Wang, Y.; Man, T.; Zhou, L.; Fang, X.; Pei, H.; Chi, L.; Liu, J. *Anal. Chem.* **2016**, *88* (23), 11684−11690.

(18) Bailo, E.; Deckert, V. *Angew. Chem., Int. Ed.* **2008**, *47* (9), 1658−61.

(19) Su, M.; Liu, H. *Nanotechnol. Environ. Sci.* **2018**, 473−514.

(20) Yu, F.; Su, M.; Tian, L.; Wang, H.; Liu, H. *Anal. Chem.* **2018**, *90* (8), 5232−5238.

(21) Zhou, B.; Mao, M.; Cao, X.; Ge, M.; Tang, X.; Li, S.; Lin, D.; Yang, L.; Liu, J. *Anal. Chem.* **2018**, *90* (6), 3826−3832.

(22) Chang, H.; Kang, H.; Ko, E.; Jun, B.-H.; Lee, H.-Y.; Lee, Y.-S.; Jeong, D. H. *ACS Sensors* **2016**, *1* (6), 645−649.

(23) Kamil Reza, K.; Wang, J.; Vaidyanathan, R.; Dey, S.; Wang, Y.; Trau, M., Electrohydrodynamic-Induced SERS Immunoassay for Extensive Multiplexed Biomarker Sensing. *Small* **2017**, *13* (9).

(24) Meyer, R.; Yao, X.; Deckert, V. *TrAC, Trends Anal. Chem.* **2018**, *102*, 250−258.

(25) Su, J.; Wang, D.; Norbel, L.; Shen, J.; Zhao, Z.; Dou, Y.; Peng, T.; Shi, J.; Mathur, S.; Fan, C.; Song, S. *Anal. Chem.* **2017**, *89* (4), 2531−2538.

(26) He, Y.; Yang, X.; Yuan, R.; Chai, Y. *Anal. Chem.* **2017**, *89* (5), 2866−2872.

(27) He, Y.; Yang, X.; Yuan, R.; Chai, Y. *Anal. Chem.* **2017**, *89* (16), 8538−8544.

(28) Zhou, W.; Tian, Y.-F.; Yin, B.-C.; Ye, B.-C. *Anal. Chem.* **2017**, *89* (11), 6120−6128.

(29) He, H.; Zhao, Z.; Han, F.; Liu, X.; Wang, R.; Zeng, Y. *Cell Death Dis.* **2016**, *7* (1), e2056.

(30) Toldo, S.; Abbate, A. *Nat. Rev. Cardiol.* **2018**, *15* (4), 203.

(31) Bansal, S. S.; Ismahil, M. A.; Goel, M.; Patel, B.; Hamid, T.; Rokosh, G.; Prabhu, S. D. *Circ.: Heart Failure* **2017**, *10* (3), e003688.

(32) Cheng, F.-Y.; Chen, C.-T.; Yeh, C.-S. *Nanotechnology* **2009**, *20* (42), 425104.

(33) Liu, Z.; Yang, Z.; Peng, B.; Cao, C.; Zhang, C.; You, H.; Xiong, Q.; Li, Z.; Fang, J. *Adv. Mater.* **2014**, *26* (15), 2431−2439.

(34) Liu, Z.; Cheng, L.; Zhang, L.; Yang, Z.; Liu, Z.; Fang, J. *Biomaterials* **2014**, *35* (13), 4099−4107.

DOI: 10.1021/acs.analchem.8b03067
Anal. Chem. 2018, 90, 11614−11621

(35) Zeng, J.; Li, M.; Liu, A.; Feng, F.; Zeng, T.; Duan, W.; Li, M.; Gong, M.; Wen, C.-Y.; Yin, Y. *Adv. Funct. Mater.* **2018**, *28*, 1800515.
(36) Garcia-Leis, A.; Torreggiani, A.; Garcia-Ramos, J. V.; Sanchez-Cortes, S. *Nanoscale* **2015**, *7* (32), 13629−37.
(37) Jenkins, S. V.; Gohman, T. D.; Miller, E. K.; Chen, J. *J. Chem. Educ.* **2015**, *92* (6), 1056−1060.
(38) Yang, Y.; Zhang, Q.; Fu, Z. W.; Qin, D. *ACS Appl. Mater. Interfaces* **2014**, *6* (5), 3750−7.
(39) Noh, M. S.; Lee, S.; Kang, H.; Yang, J. K.; Lee, H.; Hwang, D.; Lee, J. W.; Jeong, S.; Jang, Y.; Jun, B. H.; Jeong, D. H.; Kim, S. K.; Lee, Y. S.; Cho, M. H. *Biomaterials* **2015**, *45*, 81−92.
(40) Wang, X.; Ma, G.; Li, A.; Yu, J.; Yang, Z.; Lin, J.; Li, A.; Han, X.; Guo, L. *Chem. Sci.* **2018**, *9* (16), 4009−4015.
(41) Guven, B.; Dudak, F. C.; Boyaci, I. H.; Tamer, U.; Ozsoz, M. *Analyst* **2014**, *139* (5), 1141−1147.
(42) Wang, Z.; Zong, S.; Wu, L.; Zhu, D.; Cui, Y. *Chem. Rev.* **2017**, *117* (12), 7910−7963.
(43) Wang, H. N.; Crawford, B. M.; Fales, A. M.; Bowie, M. L.; Seewaldt, V. L.; Vo-Dinh, T. *J. Phys. Chem. C* **2016**, *120* (37), 21047−21055.
(44) Crawford, B. M.; Wang, H.-N.; Fales, A. M.; Bowie, M. L.; Seewaldt, V. L.; Vo-Dinh, T. In SERS-based inverse molecular sentinel (iMS) nanoprobes for multiplexed detection of microRNA cancer biomarkers in biological samples. In *Plasmonics in Biology and Medicine XIV*; International Society for Optics and Photonics: Bellingham, WA, 2017; Vol. *1008008*.
(45) Schechinger, M.; Marks, H.; Locke, A.; Choudhury, M.; Cote, G. *J. Biomed. Opt.* **2018**, *23* (1), 017002.
(46) Tabakman, S. M.; Chen, Z.; Casalongue, H. S.; Wang, H.; Dai, H. *Small* **2011**, *7* (4), 499−505.
(47) Xu, Q.; Ma, F.; Huang, S. Q.; Tang, B.; Zhang, C. Y. *Anal. Chem.* **2017**, *89* (13), 7077−7083.
(48) Sun, Y.; Peng, P.; Guo, R.; Wang, H.; Li, T. *Biosens. Bioelectron.* **2018**, *104*, 32−38.
(49) Nam, J. M.; Oh, J. W.; Lee, H.; Suh, Y. D. *Acc. Chem. Res.* **2016**, *49* (12), 2746−2755.
(50) Han, Q.; Zhang, C.; Gao, W.; Han, Z.; Liu, T.; Li, C.; Wang, Z.; He, E.; Zheng, H. *Sens. Actuators, B* **2016**, *231*, 609−614.
(51) Austin, L. A.; Mackey, M. A.; Dreaden, E. C.; El-Sayed, M. A. *Arch. Toxicol.* **2014**, *88* (7), 1391−1417.
(52) Liu, Z.; Yang, Z.; Peng, B.; Cao, C.; Zhang, C.; You, H.; Xiong, Q.; Li, Z.; Fang, J. *Adv. Mater.* **2014**, *26* (15), 2431−2439.
(53) Xu, J.; Zhao, J.; Evan, G.; Xiao, C.; Cheng, Y.; Xiao, J. *J. Mol. Med.* **2012**, *90* (8), 865−875.

DOI: 10.1021/acs.analchem.8b03067
Anal. Chem. 2018, 90, 11614−11621